The role of pyrazine-N,Nô-dioxide in $[W(CN)_8]^{n-}$-based hybrid networks: anion-´ interactions

Robert Podgajny,[a*] Dawid Pinkowicz,[a] Bernard Czarnecki,[a] Marcin Kozieğ[a] Szymon ChorÑÕy,[a] Magdalena Wis, Wojciech Nitek,[a] MichağRams[b] and Barbara Sieklucka[a]

Supporting information

Table of Content

Table 1. Ligand-assisted magnetic functionalities in the most recent $[M(CN)_8]$-based assemblies

Formula [a]	Ligand role	Magnetic features and functionality	Refs.
$[\{Mn^{II}(pyz)(H_2O)_2\}\{Mn^{II}(H_2O)_2\}\{Nb^{IV}(CN)_8\}]\cdot 4H_2O$	Bridging, 1D organic connectivity, 3D supramolecular isomerism	3D magnet, pyroelectric ferrimagnet, high MSHG/SHG ratio below T_c = 48 K	S1
Ŭ-$\{[Mn^{II}(H_2O)(urea)_2]_2[Nb^{IV}(CN)_8]\}_n$	Blocking, high dipolar moment, 3D supramolecular isomerism	3D magnetic chiral polymorh from spontaneous resolution, high MSHG/SHG signal ratio below T_c = 43K, hydration/dehydration tuned T_c 43 K Ÿ 70 K Ÿ 47 K	S2
$\{[Fe((\pm)\text{-}4\text{-}Brpy)_4]_2[Nb(CN)_8]\cdot 2H_2O\}_n$	Blocking monodentate	Chiral photomagnets from spontaneous resolution; thermally controlled Fe^{II}-centred SCO, electronic absorption, space group and SHG (1064 nm Ÿ 532 nm) intensity; optical control of magnetically ordered phases (T_c = 15 K ź 12 K) and resulting polarisation plane of MSHG signal.	S3
$\{[Mn^{II}(pydz)][Mn^{II}][Nb^{IV}(CN)_8]\}_n$	Blocking monodentate, mobile upon structural changes	3D magnet, magnetic sponge with reversible two step tuning of T_c 43 ź 68 ź 100K	S4
$\{[Ni(cyclam)]_3[W(CN)_8]_2\}_n$	Blocking, cyclic equatorial tetradentate	The honeycomb with reversible guest induced change of magnetic ordering T_c = 4.9 K (none), 8.3 K (H_2O) and 11.4 K (MeOH)	S5
$\{[Mn^{II}_2(4,4ô\text{-}bpdo)(H_2O)_4][Nb^{IV}(CN)_8]\cdot 6H_2O\}_n$	Bridging (ε-4,4ô,4ô), combination of end-to-end and end-on modes	Pillared spin-flop antiferromagnet below T_c = 15 K, magnetic phase diagram determined from monocrystalline magnetic measurements, anisotropy field of 21 kOe originating from symmetry and orientation of $[Nb(CN)_8]^{4-}$	S6
$\{Co^{II}_9(MeOH)_{24}[W^V(CN)_8]_6\}\cdot 4,4Nj\text{-}bpdo\cdot MeOH\cdot 2H_2O$ $\{Co^{II}[Co^{II}(4,4Nj\text{-}bpdo)_{1.5}(MeOH)]_8[W^V(CN)_8]_6\}\cdot 2H_2O$	Hydrogen bonded or bridging (ε-4,4ô), supramolecular isomerism	Change in magnetic relaxation correlated with modification of cluster coordination core	S7
$\{Co^{II}_3(2,2ô\text{-}bpdo)_4(H_2O)_4[W^V(CN)_8]_2\cdot 8H_2O\}$	Blocking, 7-membered coordination rings	Layered low-dimensional ferromagnet, T_c = 5.9 K, magnetic structure of monolayer simulated from the local anisotropy determined by *ab initio* calculations for Co(II) moieties	S8
$\{[Co^{II}((S,S/R,R)\text{-iPr-Pybox})(MeOH)]_3[W^V(CN)_8]_2\cdot 5.5MeOH\cdot 0.5H_2O\}_n$	Blocking, chiral, *mer*-tridentate	Chiral magnetic chains with slow magnetic relaxation, monocrystalline bulk magnetic anisotropy correlated with local axes of Co(II)	S9
$[\{(H_2O)Fe(L^1)\}\{Nb(CN)_8\}\{Fe(L)\}]_n$	Blocking, favoring the required 7-coordination bipyramidal Fe^{II} complex	Slow magnetic relaxation, magnetic hysteresis loop in 1 K, æ/k_B = 74 K Ú$_0$ = 4.6×10^{-11}s	S10
$\{[Cu_3Tb(L^{Pr})W(CN)_8(DMF)_3(H_2O)_3]\cdot(DMF)_{1.5}\cdot(H_2O)_{0.5}\}_n$	Compartmental, implying the triangular multidirectional $\{Cu_3Tb\}$ array	Coexistence of magnetic ordering, due to bridging of $\{Cu_3Tb\}$ by $[W(CN)_8]^{3-}$, and intrinsic slow magnetic relaxation in $\{Cu_3Tb\}$	S11
{æ/ş -$[Mn^{II}(S/R\text{-mpm})_2]_2[Nb^{IV}(CN)_8]\cdot 4H_2O\}_n$	Chiral, bis-chelating	Ligand directed layered chiral ferrimagnets, T_c = 23.5 K, coexistence of natural optical acitvity (NOA) and magnetic optical activity (MOA)	S12
$\{Co^{II}_3Fe^{II}_6[W^V(CN)_8]_6(MeOH)_{24}\}\cdot xMeOH$	Blocking	Trimetallic clusters, single crystal to single crystal transformation assisted by charge transfer and spin transition ($T_{ź}$ = 192 K, $T_{ŷ}$ = 205 K) through two different electron transfer channels W-CN-Co and W-CN-Fe	S13
$\{[Co^{II}(4\text{-Mepy})(pym)]_2[Co^{II}(H_2O)_2][W^V(CN)_8\}_2]\cdot 4H_2O\}_n$	Blocking (4-Mepy), Bridging (pym)	3D photomagnet, charge-transfer-induced spin transition ($T_{ź}$ = 172 K, $T_{ŷ}$ = 241 K), photoswitchable hard magnet (T_c = 48, H_{coer} = 2,7 T)	S14
$[Co^{II}(bik)_3]\{[W(CN)_8]_3[Co(bik)_2]_3\}\cdot 2H_2O\cdot 13CH_3CN$	Blocking, bis-chelating	Mixed valence decorated square, gradual charge-transfer-induced spin transition (300-150 K, T_c = 215 K), photoswitchable ground state	S15

Abbreviations: pyr = pyrazine; 4-Brpy = 4-bromopyridine; pydz = pyridazine; cyclam = 1,4,8,11-tetraazacyclotetradecane; 4,4ô-bpdo = 4,4ô-bipyridyl-N,Nô-dioxide; 2,2ô-bpdo = 2,2ô-bipyridyl-1,1ô-dioxide; iPr-Pybox = 2,2Nj(2,6-pyridinediyl)bis(4-isopropyl-2-oxazoline); L^1 pentadentate macrocycle, N,Nô-propylenebis(3-methoxysalicylideneiminato); L^{Pr} = multicompartmental ligand; mpm = Ŭ-methyl-2-pyridine-methanol; 4-Mepy = 4-methylpyridine; pym = pyrimidine; bik = bis(1-methylimidazol-2-yl)ketone.

Table S2. IR spectra of **1-5**, $Na_3[W^V(CN)_8]\cdot 4H_2O$, $K_3[W^V(CN)_8]\cdot 1.5H_2O$ and $K_4[W^{IV}(CN)_8]\cdot 2H_2O$ in the selected regions.

Compound	**Stretching C≡N (2200-2100 cm^{-1})**	**stretching (N-O) (1320-1220 cm^{-1}), C=C and C=N ring deformations (1500-1430 cm^{-1}) and C-H ring deformations (1300-1170 cm^{-1}, 1100-1000 cm^{-1} and 900-800 cm^{-1})**
1	2148m	1477s, 1461s, 1450s, 1309m, 1292m, 1261vs, 1232s(sh), 1173m, 1080w, 1055s, 946w, 860s, 810vs
2	2139m	1483s, 1465vs, 1444s(sh), 1311w, 1263vs, 1085m, 1051vs, 848s, 813vs
3	2174m, 2150m, 2132w	1477s, 1451s, 1314m, 1251m, 1236m, 1184vw, 1082w, 1053s, 878m, 848m, 811vs
4	2169w(sh), 2148m(sh), 2132s, 2124s	1477m, 1454s, 1311vw, 1294w, 1248m, 1233m, 1186w, 1084w, 1056m, 850m, 807s
5	not essential in this case	1481m, 1456s, 1314vw, 1289w, 1248m, 1233m, 1190w, 1090w, 1056m, 849m, 811s
pzdo	-	1481m, 1445vs, 1385w, 1307w, 1259vs, 1183w, 1031s, 897vw, 870m, 803vs
$K_3[W^V(CN)_8]\cdot 1.5H_2O$	2151vs, 2148vs	-
$Na_3[W^V(CN)_8]\cdot 4H_2O$	2160vs, 2154vs, 2144m	-
$K_4[W^{IV}(CN)_8]\ 2H_2O$	2130vs, 2125vs	-

Table S3. The selected bond distances [Å] and angles [deg] in **1-4.**

1			
Na1		**Na2**	
Na-O($_{pzdo}$)	2.318(3)-2.463(3) av. 2.411	Na-O($_{pzdo}$)	2.385(4), 2.554(4)
Na-N($_{NC}$)	2.430(4), 2.474(3)	Na-O($_{water}$)	2.498(4), 2.509(3)
Na-N-C	154.7(3) ,165.0(3)	Na-N($_{NC}$)	2.461(3), 2.585(3)
Na···W$_{cyano}$	5.637(2)	Na-N-C	156.8 (3), 162.5(3)
Na-O-N$_{pzdo}$	121.5(2)-134.7(2), av. 126.0	Na···W$_{cyano}$	5.761(2)
		Na-O-N$_{pzdo}$	133.3(2), 141.5(2)
Na3		**W1**	
Na-O($_{pzdo}$)	2.282(3), 2.314(3), 2.344(4)	W-C	2.152(3)-2.175(3), av. 2.16
Na-O($_{water}$)	2.427(5), 2.800(4)	C-N	1.137(5)-1.150(5), av. 1.15
Na-N($_{NC}$)	2.368(3)	W-C-N	175.6(3)-178.9(3), av. 177.5
Na-N-C	148.67(3)		
Na···W$_{cyano}$	5.443(2)		
Na-O-N$_{pzdo}$	115.5(2), 121.7(2), 154.7(2)		
2			
K2		**K3**	
K-O($_{water}$)	2.689(3)-2.718(3) av. 2.704	K-O($_{pzdo}$)	2.720(3), 2.770(3)
K-N($_{NC}$)	3.076(4), 3.174(3)	K-N($_{NC}$)	3.024(4), 3.094(3)
K-N-C	98.0(2), 104.6(3)	K-N-C	145.7(2), 150.8(2), 167.4(3)
K···W$_{cyano}$	4.846(4)	K···W$_{cyano}$	6.099(4)
		K-O-N$_{pzdo}$	133.6(2), 138.8(2)
W1			
W-C	2.158(3)-2.174(3), av. 2.166		
C-N	1.151(5)-1.153(4), av. 1.152		
W-C-N	175.1(3)-177.6(3), av. 177.5		
3			
Mn1		**Mn2**	
Mn-O($_{MetOH}$)	2.155(5), 2.212(8), 2.219(7)	Mn-O($_{MetOH}$)	2.210(4)
Mn-N($_{NC}$)	2.178(5), 2.209(5), 2.213(5)	Mn-O($_{pzdo}$)	2.144(3), 2.157(4)
Mn-N-C	164.3(5), 166.8(5), 174.7(5)	Mn-N($_{NC}$)	2.163(6), 2.193(5), 2.208(5)
Mn···W$_{cyano}$	5.459(2), 5.459(2), 5.472(2)	Mn-N-C	165.7(5), 171.1(5), 176.4(5)
		Mn···W$_{cyano}$	5.436(1), 5.469(1), 5.476(2)
		Mn-O-N$_{pzdo}$	123.9(3), 128.5(3)
Mn3		**Mn4**	
Mn-O($_{MetOH}$)	2.232(3)	Mn-O($_{MetOH}$)	2.183(6), 2.189,(6) 2.201(5)
Mn-O($_{pzdo}$)	2.122(4), 2.171(4)	Mn-N($_{NC}$)	2.212(5), 2.216(5), 2.225(5)
Mn-N($_{NC}$)	2.142(6), 2.180(5), 2.227(5)	Mn-N-C	168.0(5), 173.1(5), 175.5(5)
Mn-N-C	166.4(5), 170.6(5), 176.1(5)	Mn···W$_{cyano}$	5.487(2), 5.492(2), 5.522(2)
Mn···W$_{cyano}$	5.411(1), 5.481(1), 5.487(2)		
Mn-O-N$_{pzdo}$	124.9(3), 129.4(3)		

Mn5		**Mn6**	
Mn-O($_{MetOH}$)	2.234(4)	Mn-O($_{MetOH}$)	2.212(4)
Mn-O($_{pzdo}$)	2.170(4), 2.195(4)	Mn-O($_{pzdo}$)	2.150(4), 2.182(4)
Mn-N($_{NC}$)	2.182(5), 2.225(6), 2.232(5)	Mn-N($_{NC}$)	2.195(4), 2.196(5), 2.233(5)
Mn-N-C	158.9(5), 171.6(5), 177.7(5)	Mn-N-C	148.2(5), 159.2(5), 169.4(5)
Mn···W$_{cyano}$	5.451(2), 5.470(1), 5.524(1)	Mn···W$_{cyano}$	5.467(2), 5.472(1), 5.494(1)
Mn-O-N$_{pzdo}$	129.0(3), 129.2(3)	Mn-O-N$_{pzdo}$	130.2(3), 131.1(4)
W1		**W2**	
W-C	2.165(5)-2.204(6), av. 2.177	W-C	2.136(5)-2.164(6), av. 2.172
C-N	1.108(8)-1.144(9), av. 1.129	C-N	1.137(7)-1.157(8), av. 1.145
W-C-N	177.5(5)-178.8(6), av. 177.9	W-C-N	174.8(5)-179.0(5), av. 178.8
W3		**W4**	
W-C	2.152(5)-2.174(5), av. 2.165	W-C	2.152(5)-2.174(5), av. 2.159
C-N	1.119(8)-1.152(9), av. 1.138	C-N	1.131(8)-1.153(7), av. 1.144
W-C-N	175.1(5)-179.4(5), av. 177.9	W-C-N	175.7(5)-179.2(5), av. 178.1
4			
Mn		**W**	
Mn-O($_{water}$)	2.208(2), 2.184(2)	W-C	2.155(3)-2.172(3), av. 2.162
Mn-O($_{pzdo}$)	2.252(2)	C-N	1.148(5)-1.155(3), av. 1.152
Mn-N($_{NC}$)	2.204(2), 2.216(2), 2.196(2),	W-C-N	178.1(4)-179.9(2),av.178.77
Mn-N-C	171.1(2), 171.5(2), 176.0(2)		
Mn···W$_{cyano}$	5.518(3)		
Mn-O-N$_{pzdo}$	117.2(2)		

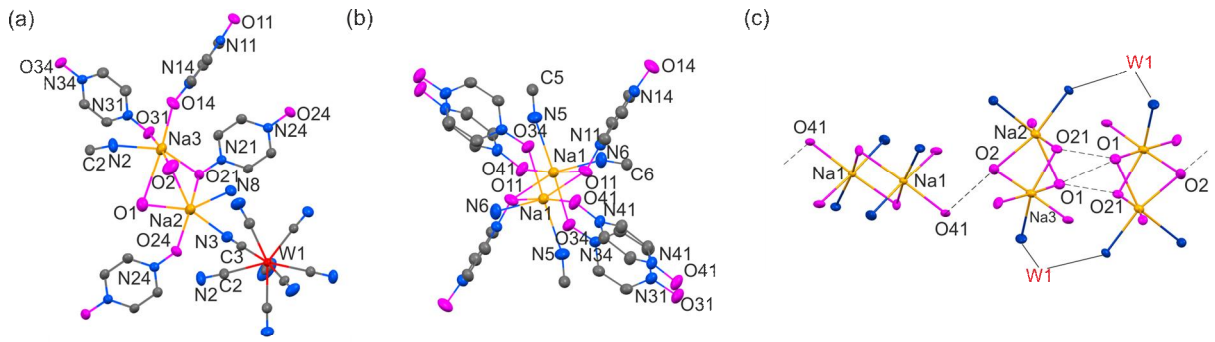

Figure S1. The illustration of the crystal structure of **1** with the atom numbering scheme (a,b). Hydrogen bonding between $\{Na_2O_3\}$ and $\{N_2O_2\}$ nodes (c).

SHAPE calculations

Shape measures analysis suggest strongly that the coordination sphere of W in **1**, **2** and **4** is very close to SAPR-8 due to low values of S_{SAPR} in comparison to S_{DD} and S_{JBTP}. In **3,** two of tungsten atoms have coordination sphere of slightly-distorted square antiprismatic geometry (W2 and W3) and other two have the shape of slightly-distorted triangular dodecahedron (W1 and W4). All manganese coordination spheres (both in **3** and **4**) possess a slightly distorted octahedral geometry, with S_{OC} values smaller than 1 and significantly smaller than S_{TP} values. Results of calculations are presented in Table S4 for tungsten atoms and S5 for manganese atoms.

Table S4. Continuous Shape Measure (CShM) Analysis[a] for the coordination spheres of W in **1-4**

	W (1)	**W (2)**	**W1 (3)**	**W2 (3)**	**W3 (3)**	**W4 (3)**	**W (4)**
S_{SAPR}	0.344	0.473	0.344	1.662	1.905	0.279	0.511
S_{DD}	1.625	1.438	1.625	0.322	0.272	1.790	1.880
S_{JBTP}	2.310	2.336	2.310	2.605	2.743	2.366	2.078

* square antiprism, ** triangular dodecahedron, *** biaugmented trigonal prism

[a] S_{SAPR}, S_{DD}, S_{JBTP} ï continuous shape measures related to the SAPR-8, DD-8, JBTP-8 geometry, respectively (equal to 0 if the real geometry coincides with the idealized one)

Table S5. Continuous Shape Measure (CShM) Analysis[a] for the coordination spheres of Mn^{II} in **3** and **4**

	Mn1 (3)	**Mn2 (3)**	**Mn3 (3)**	**Mn4 (3)**	**Mn5 (3)**	**Mn6 (3)**	**Mn (4)**
S_{OC}	0.433	0.443	0.652	0.179	0.877	0.907	0.181
S_{TP}	13.767	13.465	12.738	15.387	12.449	12.445	15.098

* octahedron, ** trigonal prism

[a] S_{OC}, S_{TP} ï continuous shape measure relatied to the OC-6 and TP-6 geometry, respectively (equal to 0 if the real geometry coincides with the idealized one);

Magnetic properties.

Compounds **1** and **2** in the 50 ï 300 K temperature range have constant χT = 0.37 cm^3ÃKÃmol^{-1} per tungsten(V) center, which is very close to the expected spin-only value of 0.375 cm^3ÃKÃmol^{-1} for S = ½ and assuming isotropic g = 2.0 (Figure S2). Below T = 50 K the $\chi T(T)$ dependence starts to decrease reaching at 2 K the values of 0.34 (**1**) and 0.28 (**2**) cm^3ÃKÃmol^{-1}. Such behavior might indicate a weak antiferromagnetic interactions or significant anisotropy of $[W^V(CN)_8]^{3-}$.

Fitting the $\chi T(T)$ dependence using the mean-field approximation

$$\chi = \chi_0 /(1-\frac{2zJ'}{Ng^2\beta^2}\chi_0)$$,

where χ_0 denotes susceptibility of a separated S = 1/2 spin and zJ' describes an antiferromagnetic interactions between W^V ions, we obtained g_w = 1.98 and zJ' = -0.196 cm^{-1} for **1** and g_W = 1.98 and zJ' = -0.455 cm^{-1} for **2**.

For both compounds the $M(H)$ curves are close to the Brillouin functions for S = 1/2 and g = 1.98 (Figure S3), which is in line with the aforementioned fitting results.

The compound **4** behave as a paramagnet due to the presence of very weakly coupled paramagnetic Mn^{II} centers. The measured high temperature χT limit of 8.7 cm^3ÃKÃmol^{-1} (Figure S7) is in agreement with 8.75 cm^3ÃKÃmol^{-1} expected for two isolated Mn^{II} ions (S = 5/2, g = 2.0). With the decreasing temperature the signal is almost constant down to ~100 K. Below this point it starts to decrease very slowly. The decrease of the signal becomes pronounced below 25 K. At T = 2 K the χT product is 3 cm^3ÃKÃmol^{-1}. Using the approximation similar as in case of **1** and **2**, the best-fit parameters: g_{Mn} = 2.04 and zJ' = -0.091 cm^{-1} were obtained for **4**.

The M is a linear function of H up to 20 kOe and begins to saturate very slowly above this point to reach a value of 8.2 Nß at H = 50 kOe which is much below the expected 10 Nß (for two Mn^{II} centers assuming S = 5/2 and g = 2.0). The $M(H)$ runs much lower than the sum of 2 Brillouin functions for S = 5/2 and g = 2.04 (Figure S8). The Mn^{II}ÃÃÃMn^{II} distances in the Mn^{II}-NC-W^{IV}-CN-Mn^{II} linkage are within the range 6.9-10.7 Å, the lowest limit being also the Mn^{II}ÃÃÃMn^{II} distance within Mn^{II}-pzdo-Mn^{II} linkage. The magnetic interactions Mn-Mn could operate through the diamagnetic $[W(CN)_8]^{4-}$ bridges or through the pzdo bridges.

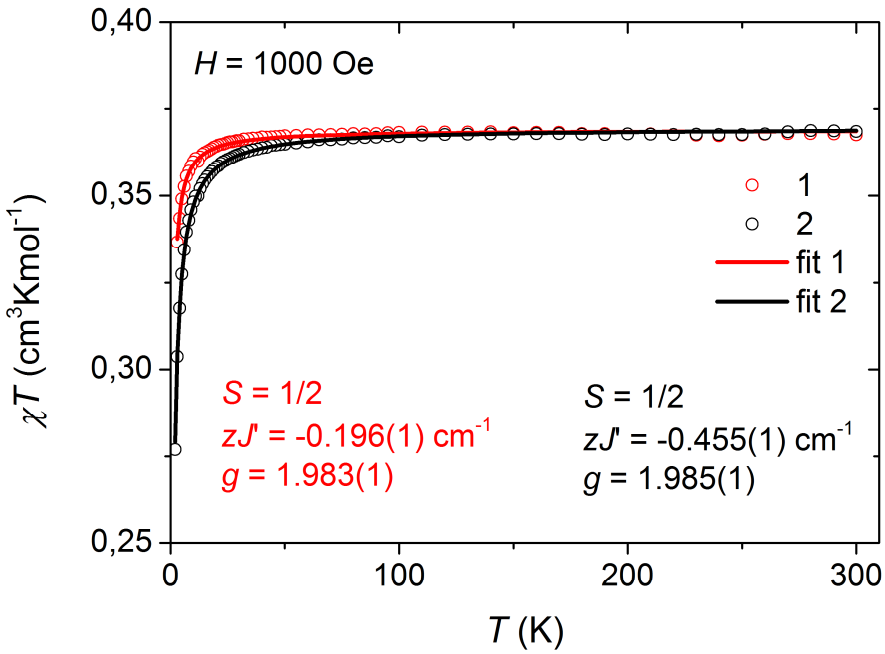

Figure S2. Magnetic properties of **1** (red) and **2** (black). $\chi T(T)$ at H = 1 kOe. Solid lines represent the best fit to the experimental data (see text above for details).

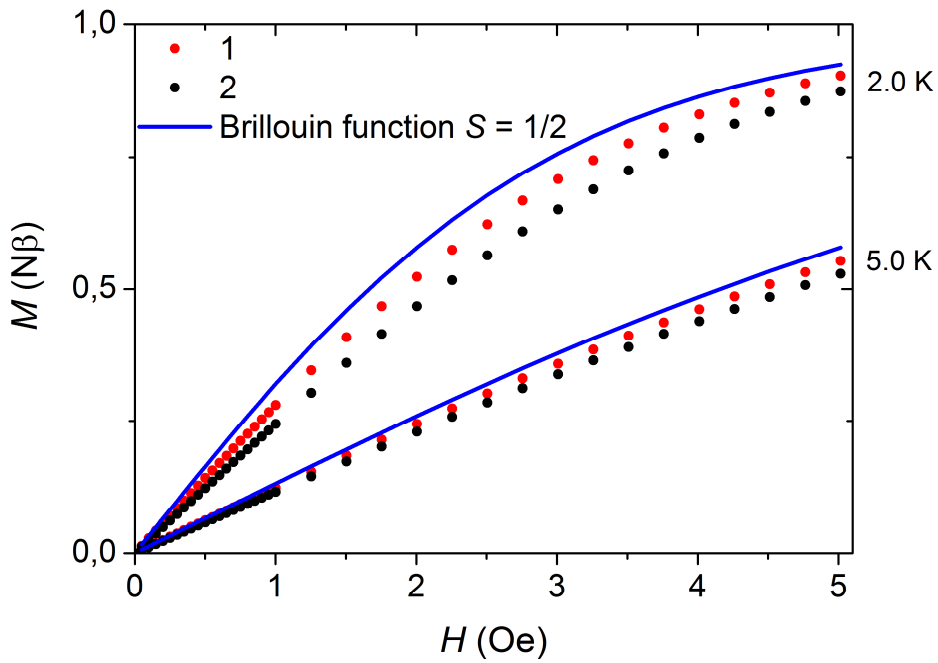

Figure S3. $M(H)$ curves for **1** (red) and **2** (black) at T = 2 K and T = 5 K. The blue solid lines show the Brillouin functions for spin S = 1/2 and g = 1.98.

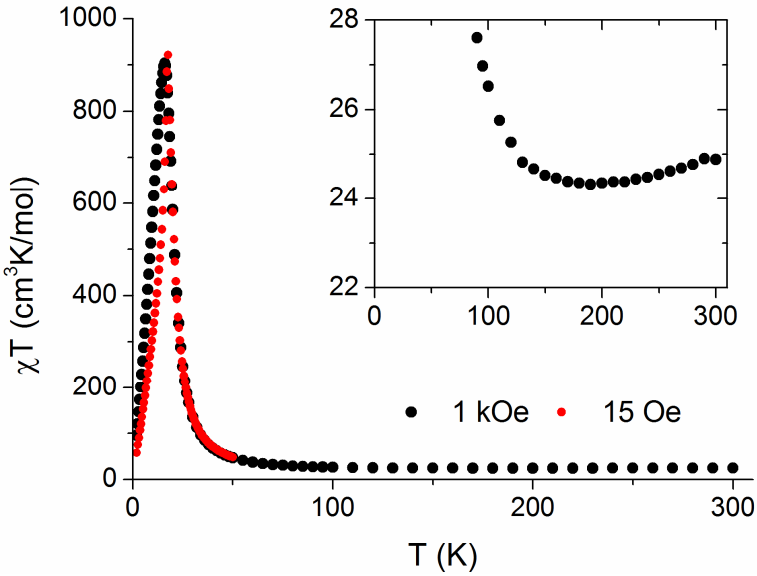

Figure S4. Magnetic susceptibility temperature product for **3** from measurements made at 1 kOe (black points) and at 15 Oe (red points). In the inset: enlarged high temperature part.

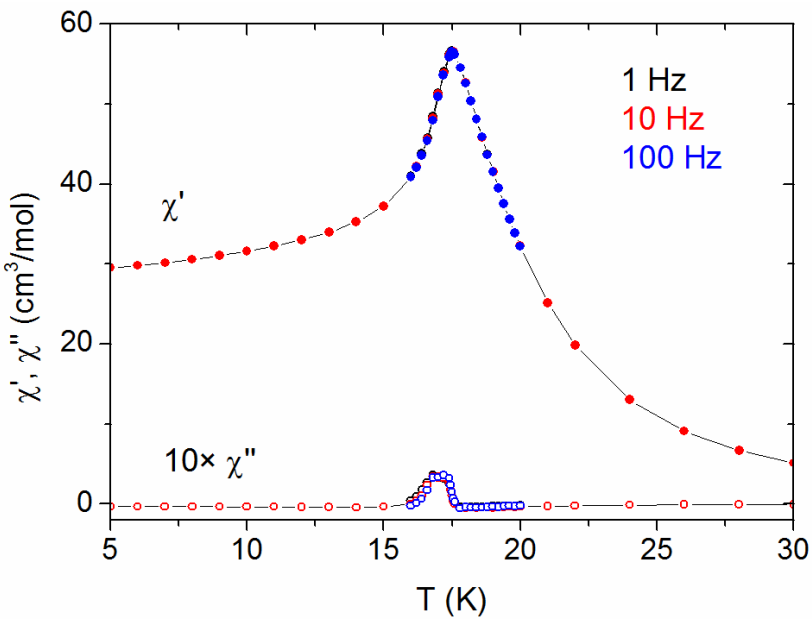

Figure S5. Magnetic properties of **3**: ac magnetic susceptibility $\chi'(T)$ and $\chi''(T)$ curves measured using different ac frequencies. The χ'' data are multiplied 10 times to be visible. No shift in the position of the peak is detected.

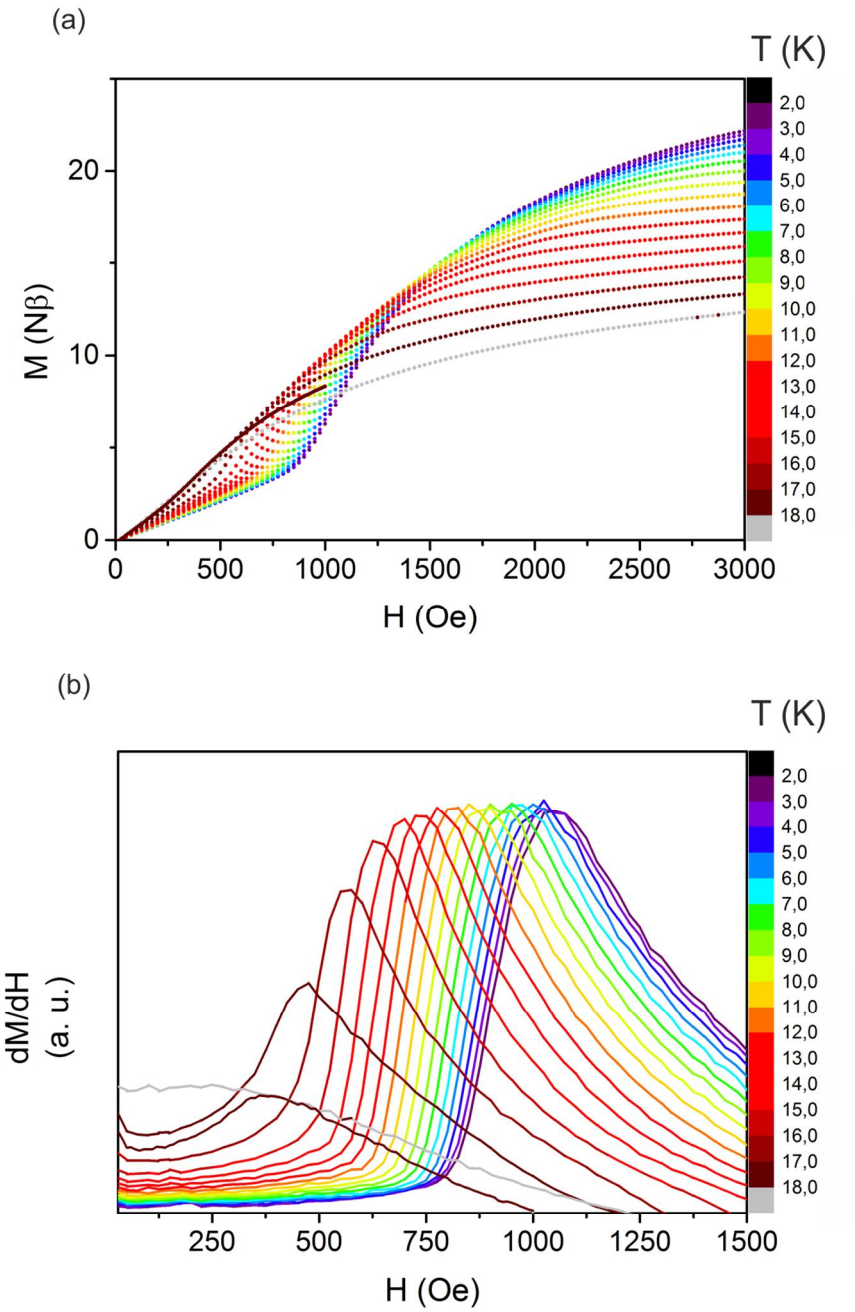

Figure S6. Magnetic properties of **3**: the complete set of *M*(*H*) dependencies (a) and the relevant d*M*/d*H*(*H*) dependencies (b) at *T* range 2 ï 18 K, according to the vertical coloration scale). The maxima of d*M*/d*H*(*H*) were used for magnetic phase diagram determination.

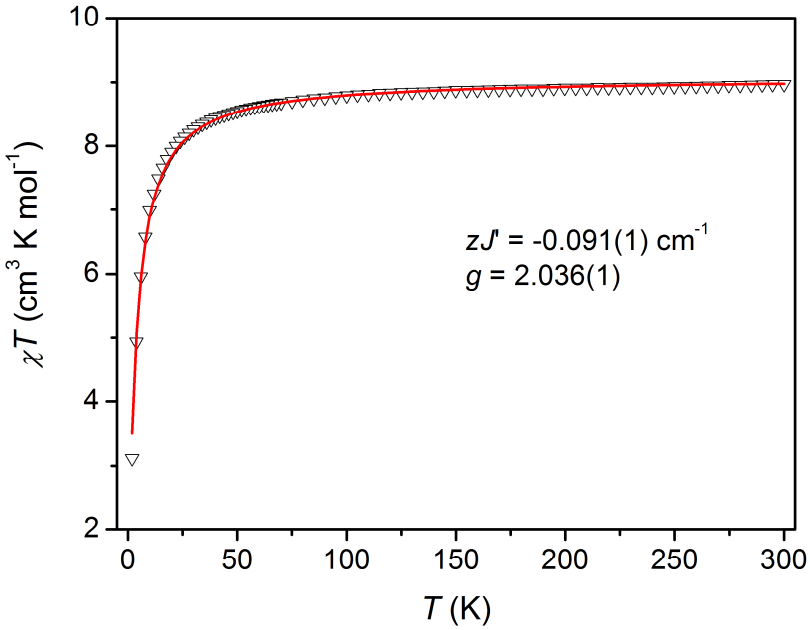

Figure S7. Temperature dependence $\chi T(T)$ at H = 1 kOe calculated for Mn_2W unit for **4**. Red solid line is the best fit to the experimental data.

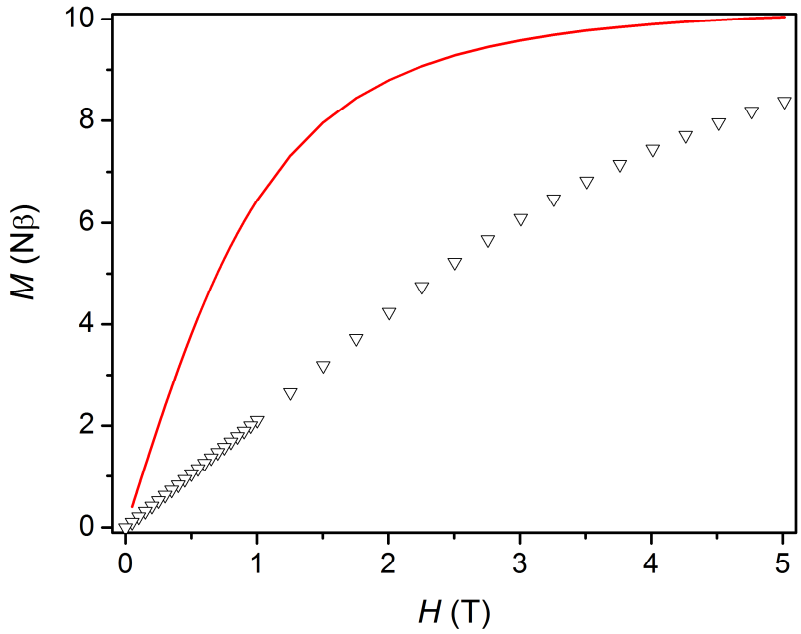

Figure S8. Field dependent magnetization $M(H)$ at T = 2 K for **4**. The red solid line shows the Brillouin function for two uncoupled spins S = 5/2 and g = 2.04.

Literature

(S1) Tsunobuchi, Y.; Kosaka, W.; Nuida, T.; Ohkoshi, S. *CrystEngComm*, **2009**, *11*, 2051ï 2053.

(S2) Pinkowicz, D.; Podgajny, R.; Nitek, W.; Rams, M.; Majcher, A. M.; Nuida, T.; Ohkoshi, S.; Sieklucka, B. *Chem. Mater.* **2011**, *23*, 21ï 31.

(S3) Ohkoshi, S.; Takano, S.; Imoto, K.; Yoshikiyo, M.; Namai, A.; Tokoro, H. *Nat. Photon.* **2013**, 8, 65-71.

(S4) Pinkowicz, D.; Podgajny, R.; Gaweğ B.; Nitek, W.; Ğasocha, W.; Oszajca, M.; Czapla, M.; Makarewicz, M.; Bağanda, M.; Sieklucka, B., *Angew. Chem. Int.Ed.* **2011**, *50*, 3973ï 3977.

(S5) Nowicka, B.; Bağanda, M.; Gaweğ B.; Cwiak, G.; Budziak, A.; Ğasocha, W.; Sieklucka, B. *Dalton Trans.*, **2011**, *40*, 3067-3073.

(S6) Pinkowicz, D.; Rams, M.; Nitek, W.; Czarnecki, B.; Sieklucka, B. *Chem.Comm.*, **2012**, *48*, 8323-8325.

(S7) Chorazy, S.; Podgajny, R.; Nitek, W.; Rams, M.; Ohkoshi, S.; Sieklucka, B. *Cryst. Growth Des.* **2013**, *13*, 3036-3045.

(S8) Chorazy, S.; Podgajny, R.; Majcher, A. M.; Nitek, W.; Rams, M.; Suturina, E. A.; Ungur, L.; Chibotaru, L. F.; Sieklucka, B. *CrystEngComm* **2013**, *15*, 2378ï 2385.

(S9) Chorazy, S.; Nakabayashi, K.; Imoto, K.; Mlynarski, J.; Sieklucka, B.; Ohkoshi, S. *J. Am. Chem. Soc.* DOI: 10.1021/ja307520k.

(S10) Venkatakrishnan, T. S.; Sahoo, S.; Brefuel, N.; Duhayon, C.; Paulsen, C.; Barra, A.-L.; Ramasesha, S.; Sutter, J.-P.; *J. Am. Chem. Soc.*, **2010**, *132*, 6047ï 6056.

(S11) Dhers, S.; Feltham, H. L. C.; Clérac, R.; Brooker S.; *Inorg. Chem.* **2013**, 52, 13685ï 13691.

(S12) Chorazy, S.; Podgajny, R.; Nitek, W.; Fic, T.; Görlich, E.; Rams, M.; Sieklucka, B. *Chem. Commun.*, **2013**, *49*, 6731ï 6733.

(S13) Podgajny, R.; Chorazy, S.; Nitek, W.; Rams, M.; Majcher, A. M.; Marszağek, B.; ŧ ukrowski, J.; Kapusta, C.; Sieklucka, B. *Angew. Chem. Int. Ed.* **2013**, *52*, 896ï 900.

(S14) Ozaki, N.; Tokoro, H.; Hamada, Y.; Namai, A.; Matsuda, T.; Kaneko, S.; Ohkoshi, S. *Adv. Funct. Mater.* **2012**, *22*, 2089ï 2093

(S15) Mondal, A.; Chamoreau, L.-M.; Li, Y.; Journaux, Y.; Seuleiman, M.; Lescouy zec R. *Chem. Eur. J.* **2013**, *19*, 7682ï 7685.